Hydrogeology Journal (2019) 27:2707–2718
https://doi.org/10.1007/s10040-019-02012-0

REPORT

# Assessing bare-soil evaporation from different water-table depths using lysimeters and a numerical model in the Ordos Basin, China

Zhitong Ma[1,2] · Wenke Wang[1,2] · Zaiyong Zhang[1,2] · Philip Brunner[3] · Zhoufeng Wang[1,2] · Li Chen[1,2] · Ming Zhao[1,2] · Chengcheng Gong[1,2]

Received: 11 September 2018 / Accepted: 25 June 2019 / Published online: 16 July 2019
© Springer-Verlag GmbH Germany, part of Springer Nature 2019

## Abstract

In semiarid and arid regions, the evaporation from bare soil is highly sensitive to changes in the depth to the water table. This study quantifies the relation between water-table depth and the groundwater contribution to evaporation in the Ordos Basin in China. In-situ field experiments were combined with numerical simulations of heat, vapor and liquid water flow. Based on lysimeter experiments and a calibrated numerical model, a relation between depth to groundwater and evaporation rate was established for the lysimeter site. In addition, a sensitivity analysis considering the hydraulic conductivity and the inverse of the air-entry pressure (van Genuchten $\alpha$) was established. For the field site, the results showed that for the water-table depths less than 52 cm below the ground, evaporation is independent of the water-table depth. For water-table depths exceeding 52 cm, an exponential relation between depth to groundwater and evaporation is observed. No phreatic evaporation occurs for water tables deeper than 105 cm, which is nearly two times the capillary fringe height. The sensitivity analysis showed that the extinction depth decreased with decreasing hydraulic conductivity and increased with $\alpha$. The field-specific results and the sensitivity analysis provide valuable information to understand the dynamic processes of soil evaporation in the Ordos Basin. From a methodological point of view, the proposed modelling approach and the integration of lysimeter data proved to be a highly efficient combination to study evaporation dynamics in semi-arid and arid environments.

**Keywords** Soil evaporation · Extinction depth · Numerical modelling · Lysimeter · Arid-region

## Introduction

Bare soil evaporation can account for 50–70% of the total annual evaporation (Baldocchi and Xu 2007). Evaporation from bare soil is therefore critical for determining water budgets, especially in arid and semi-arid regions (Doble et al. 2006; Selim et al. 2013; Wang et al. 2017; Shah et al. 2007; Banimahd & Zand-Parsa 2013; Shang et al. 2016; Nazarieh et al. 2018). Apart from being an important component of the water balance, the contribution of groundwater to evaporation is critical to managing a range of environmental threats, for example, soil degradation through soil salinization (Hillel 1998; Brunner et al. 2007, 2008). Exploring the mechanisms of soil evaporation is therefore of great importance in arid and semi-arid areas.

The dynamics of soil evaporation are affected by various factors such as soil texture and the associated soil retention capabilities, atmospheric demand, and the water-table depth (Philip 1957; Talsma 1963; Song et al. 2014; Balugani et al. 2016). In particular, soil evaporation is strongly dependent on the water-table depth. Evaporation is either limited by atmospheric conditions or by the hydraulic properties of the porous medium—i.e. the supply of water through capillary rise (Salvucci 1997; Lehmann et al. 2008; Kamai and Assouline 2018). The water-table depth is an important factor in this regard.

In an endeavor to better understand the physical process of soil evaporation, the influence of vapor dynamics in the unsaturated zone on evaporation was studied by Ripple et al. (1970).

✉ Wenke Wang
wenkew@chd.edu.cn

[1] Present address: Key Laboratory of Subsurface Hydrology and Ecological Effects in Arid Region, Chang'an University, Ministry of Education, Chang'an, People's Republic of China

[2] School of Environmental Science and Engineering, Chang'an University, Yanta Road 126, 710054 Xi'an, Shaanxi, People's Republic of China

[3] Center for Hydrogeology and Geothermics, (CHYN), Université de Neuchâtel, Neuchâtel, Switzerland

They concluded that vapor dynamics play an important role in the evaporation process. This is in line with many other studies that conclude that the joint consideration of the soil water movement along with vapor phase processes is of critical importance to understanding evaporation processes (Nimmo et al. 2002; Walvoord et al. 2002; Scanlon et al. 2003; Balugani et al. 2017; Assouline et al. 2013). Zhang et al. (2018) investigated the bare soil evaporation in relation to water-table depths by developing coupled liquid and vapor flow solutions for a shallow water-table system and highlighted the importance of considering vapor dynamics for the assessment of soil evaporation.

There are numerous methods to estimate soil-water-evaporation rates from bare soil (Doble and Crosbie 2017), including, for example, experimental observations, analytical methods, and numerical models using the Richards equation. Over the past few decades, laboratory experiments have been conducted to identify the role of factors such as soil type, moisture content or temperature on soil evaporation (Gowing et al. 2006; Assouline et al. 2013; Kamai et al. 2009; Hernández-López et al. 2014). A pioneering study focusing on the relation between the water-table depth and evaporation rates was carried out by Gardner and Fireman (1958). Based on experiments carried out in the laboratory, they calculated that the decline of bare soil evaporation decreases exponentially with increasing water-table depths. While laboratory experiments provide critical information concerning evaporation, their applicability to field settings is not straight forward.

A range of high-precision field experiments was carried out to estimate the evaporation rates in natural conditions by Yamanaka and Yonetani 1999; Fahle and Dietrich 2014; Chen et al. 2018; Zhang et al. 2019. In addition to field and laboratory experiments, numerous modeling approaches were suggested. These include analytical solutions (Gardner 1958; Ripple et al. 1970; Sadeghi et al. 2012; Selker 2017). For example, Brutsaert (2014) deduced an analytical solution describing the temporal dynamics of the zero-flux plane depth and the rate of evaporation. Analytical solutions, however, cannot account for all the physical processes relevant to evaporation. In order to better account for flow and heat transport dynamics in the unsaturated zone, numerical models have been identified as an effective tool (Doble et al. 2006; Shah et al. 2007; Johnson et al. 2010; Wang et al. 2011b; Soylu et al. 2011; Liu et al. 2015).

The combination of modelling approaches and field observations from, e.g. lysimeters has been very successful. For example, based on lysimeter experiments and numerical simulations, Wang et al. (2011a) analyzed the water and heat movement in the unsaturated zone and showed that the extinction depth in sandy material is about 70 cm. Shah et al. (2007) assessed the influence of different soil textures on extinction depths using numerical simulations. The consideration of evaporation processes in regional-scale settings has also been receiving attention. For example, a method for emulating evapotranspiration processes in groundwater flow models was developed by Doble et al. (2017). Li et al. (2008) developed a numerical approach to account for sub-grid topographic variations in the calculation of soil-evaporation rates using the numerical model MODFLOW.

The goal of this study is to quantify the relation between the depth to groundwater and evaporation rates for the so-called "wind-blown sand area" of the Ordos Basin, China. This relation can be used in large-scale numerical models and is highly relevant to water resources management. In order to achieve these goals, this study combined long-term in-situ field observations with a numerical model simulating the liquid and vapor phases of water, as well as heat transport. Given that previous research identified vapor transport as a critical component, this study explicitly considers this process in the modelling approach. The models were calibrated using lysimeters featuring two different water-table depths. Based on the calibrated models, additional water-table depths were simulated to establish a quantitative relationship between water-table depth and evaporation rate. The models also allow for quantifying the extinction depth. Moreover, a sensitivity analysis on how the hydraulic conductivity and the inverse of the air-entry pressure ($\alpha$ in the van Genuchten equations) affect the extinction depth was carried out. While the results of the study are mainly relevant for the project area, some aspects of the chosen methodology, especially the comprehensive consideration of physical processes, can also be of interest for other project areas.

## Materials and methods

### Research site description and data collection

An in-situ field experiment (Fig. 1) was carried out at a national meteorological station located in the town of Henan of Ordos City, Inner Mongolia, northwestern China (37°51' N, 108°43′ E, 1,210 m). Two lysimeters, each with a diameter of 60 cm, were mounted at the bottom of the station, and PVC pipes with a diameter of 5 cm were inserted in the middle of both lysimeters to monitor changes of the water table. One of the lysimeters was buried 305 cm deep and the depth of the water table was around 290 cm (see Fig. 2). Here, this lysimeter is referred to as case 1, whereas the other lysimeter was buried 190 cm deep and the water-table depth varied between 0 and 80 cm. (see Fig. 2) and is referred to as case 2. The bottom ends of the two lysimeters were sealed to prevent water leakage from and to the saturated zone.

Soil water content at the depths of 3, 5, 10, 50 and 100 cm were measured using ECH2O-5TM (Decagon Inc., ±1~2%) sensors in both lysimeters, and at each depth a temperature probe was installed (An et al. 2016, 2017). In addition, the fluctuation of the water table was monitored using a DI501 mini diver (Diver Inc., ±0.05%) installed at the very bottom of each lysimeter with a pipe open to the atmosphere. All sensors were set to record data at an interval of 5 min.

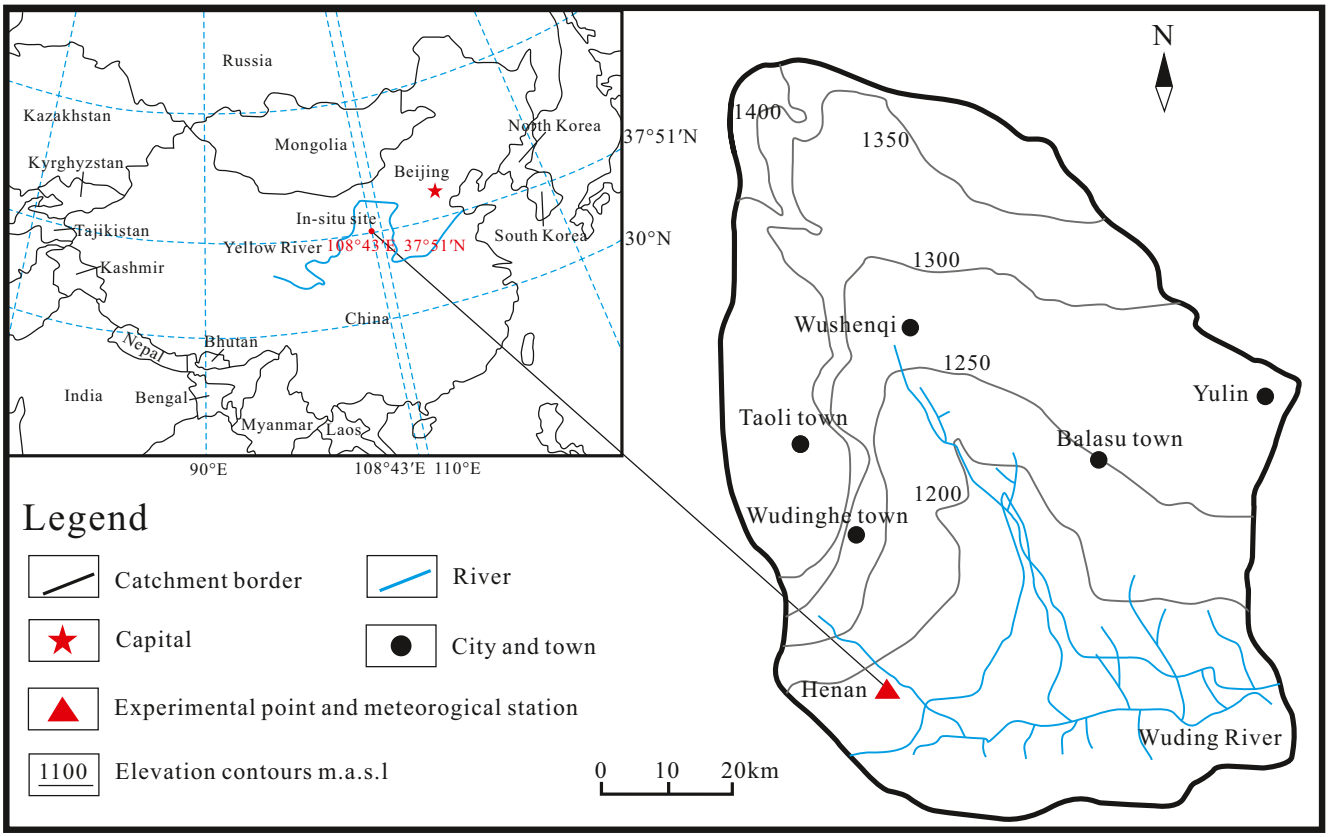


**Fig. 1** Location of the Wuding River catchment and the research site

## Meteorological data and water-table fluctuations

The parameters of maximum and minimum air temperature, relative humidity, rainfall, wind speed and net radiation at 2 m height were obtained hourly from the national meteorological station. The average annual air temperature in this region is 8.0 °C with minimum and maximum monthly averages being −32 °C in January and 36.7 °C in July. Rainfall dynamics include both heavy rainfall events and continuous rainfall of several days of small intensity. 75% of the annual rainfall occurs from July to October, and the average annual rainfall is 320 mm, while the average annual potential evapotranspiration is around 2,180 mm (Huang et al. 2015).

Figure 2 shows the fluctuation of the water table for case 1 and case 2 during the period analyzed. For case 1, the water-table depth slowly increased, and the fluctuation range was about 5.6 cm. By contrast, for case 2, the water-table depth varied more significantly and ranged from 0 to 80 cm.

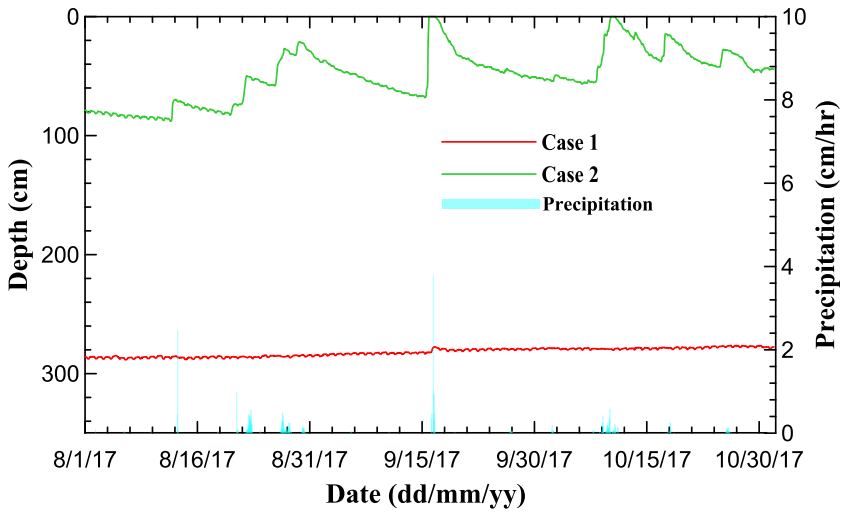


**Fig. 2** Fluctuation of the water tables and precipitation rates

### Material properties

Samples of the lysimeter material were obtained from depths of 8, 30, 50 and 100 cm. Based on these samples the following parameters were obtained: The soil water retention curve (van Genuchten parametrization), the hydraulic conductivity, grain size distribution, thermal parameters such as volumetric heat capacity of the solid ($C_n$) and liquid water ($C_w$), as well as the thermal conductivity ($\lambda$). The soil profile was composed of fine sand; the particle size distributions of the soils were obtained by the sieve method. Soil matric potential and volumetric water content were obtained by the so-called ku-pF measurement system (UGT, Germany). The van Genuchten parameters were obtained by fitting the retention curve.

## Numerical model

The model HYDRUS-1 D by U.S. Salinity Laboratory was developed for simulating water, heat and solute movement in one-dimensional (1D) variably-saturated media (Simunek 2005). It is based on the finite element method. The original model was extended by Simunek et al. (2008) to additionally simulate vapor and heat, as well as the surface energy and water balance.

### Equations for mass transport

The total moisture flux $q_m$ (cm $h^{-1}$; is given by Milly 1982):

$$q_m = q_L + q_v \tag{1}$$

where $q_L$ and $q_v$ are the flux density of liquid water and vapor, respectively (cm $h^{-1}$). $q_L$ is simulated using a modified Darcy's Law equation, as given by Philip and De Vries (1957):

$$q_L = -K_{Lh}\left(\frac{\partial h}{\partial z} + 1\right) - K_{LT}\frac{\partial T}{\partial z} \tag{2}$$

where $K_{Lh}$(cm $h^{-1}$) and $K_{LT}$ (cm$^2$ $h^{-1}$ $K^{-1}$) are the isothermal and thermal hydraulic conductivities for the liquid phase. $h$ is the pressure head (cm), $T$ is the temperature (K), z is the spatial coordinate. Water retention is characterized by the van Genuchten (1980) approach:

$$S_e = \frac{\theta - \theta_r}{\theta_s - \theta_r} \tag{3}$$

$$\frac{\theta - \theta_r}{\theta_s - \theta_r} = \frac{1}{(1 + |\alpha h|^n)^m} \tag{4}$$

$$K_{Lh}(h) = K_s S_e^l \left[1 - \left(1 - S_e^{\frac{1}{m}}\right)^m\right]^2 \tag{5}$$

where $K_s$ (cm $h^{-1}$) is the saturated hydraulic conductivity, $S_e$ is effective saturation, $h$ is the pressure head (cm), $m$ and $n$ are empirical coefficients affecting the shape of the retention functions, $l$ is a pore-connectivity parameter, and $\theta_s$ and $\theta_r$ are saturated and residual water content, respectively (cm$^3$ cm$^{-3}$).

The water vapor flux can be redefined as (Philip and De Vries 1957):

$$q_v = -K_{vT}\nabla T - K_{v\theta}\nabla\theta \tag{6}$$

where $K_{vT}$ (cm$^2$ $K^{-1}$ $h^{-1}$) and $K_{v\theta}$ (cm $h^{-1}$) are isothermal and thermal hydraulic conductivities for the vapor phase.

Evaporation $E$ (cm $h^{-1}$) from the soil surface, controlled by the atmospheric conditions and water transport, is calculated as follows:

$$E = \frac{\rho_{vs} - \rho_{va}}{r_v + r_s} \tag{7}$$

where $\rho_{vs}$ is the water vapor density at the soil surface (kg ), $\rho_{va}$ is the atmospheric vapor density (kg cm$^{-1}$), $r_v$ is the aerodynamic resistance to water vapor flow (h cm$^{-1}$), $r_s$ is the soil surface resistance to water vapor flow (h cm$^{-1}$).

### Heat transport

The governing equation for the movement of energy in the porous medium is given by Saito et al. 2006:

$$\frac{\partial S_h}{\partial t} = -\frac{\partial q_h}{\partial z} - Q \tag{8}$$

where $S_h$ is the heat stored in soil (J cm$^{-3}$), $q_h$ is the total heat flux density (J cm$^{-2}$ $h^{-1}$), and $Q$ accounts for sources and sinks of energy (J cm$^{-2}$ $h^{-1}$). The storage of heat is computed using an approach suggested by de Vries 1963:

$$S_h = C_n T\theta_n + C_W T\theta_L + C_V T\theta_V + L\theta_V \tag{9}$$

where $\theta_n$, $\theta_L$, and $\theta_V$ are volumetric fractions of solid, liquid water and water vapor phases (cm$^3$ cm$^{-3}$) respectively, $C_n$, $C_W$, and $C_V$ are volumetric heat capacities (J cm$^{-3}$ $K^{-1}$) of solid, liquid water and water vapor phases, respectively, and $T$ is the temperature (K). $L$ is the volumetric latent heat of vaporization (J cm$^{-3}$).

The total heat flux density, $q_h$, is the sensible heat as described by Fourier's law (de Vries 1958):

$$q_h = -\lambda(\theta)\frac{\partial T}{\partial z} + C_W T q_L + C_V T q_v + L q_v \tag{10}$$

where $\lambda(\theta)$ is the thermal conductivity of soil (J cm$^{-1}$ $h^{-1}$ $K^{-1}$), and $q_L$ and $q_v$ are flux of liquid water and water vapor (cm $h^{-1}$), respectively.

Thermal conductivity is conceptualized based on an approach by Chung and Horton (1987):

$$\lambda(\theta) = b_1 + b_2\theta + b_3\theta^{0.5} \quad (11)$$

where $b_1$, $b_2$, $b_3$, are empirical regression parameters.

### Model geometry, initial and boundary conditions

The model was conceptualized as a 1D column without lateral flux and surface runoff. The two simulated domains were 305 and 190 cm high, respectively. The vertical discretization is 1 cm in both cases, which is fine enough to adequately solve the Richards equation and the equations to simulate heat and vapor transport.

The initial water content and temperature of the soil profile were determined on August 1st through measurements in the lysimeters and implemented in the model. Two different sets of boundary conditions were employed, one for model calibration, and one for establishing the relation between water-table conditions and evaporation dynamics.

For model calibration, the boundary conditions are implemented as follows. The lower hydraulic boundary condition is a no-flow boundary. Atmospheric forcing at the soil surface for liquid water and water vapor and heat transport correspond to atmospheric boundary conditions. Potential evaporation is calculated using the Penman–Monteith equation (Allen et al. 1998). Precipitation is based on the measured data during the simulation period. For heat transport, the upper boundary condition was defined through a Dirichlet type condition based on the temperature measurements carried out at the field site: $T\ (0, t) = T_{\text{top}}$. The lower boundary condition was defined through a second boundary type (Neumann type): $\frac{\partial T}{\partial Z} = 0$, where 0 and $z$ represent the location of the surface soil and water table, respectively.

For the subsequent model simulations based on the calibrated model (to explore the extinction depth in relation to the hydraulic conductivity and $\alpha$), no precipitation was implemented. If precipitation would have been considered, assessing the contribution of groundwater to evaporation would have been difficult as both the infiltrating precipitation and rising groundwater will contribute to evaporation. The annual average of the Penman–Monteith equation was used for potential evaporation.

### Model calibration

The model was calibrated by comparing model simulations with measured water content and soil temperature. All available observations were included in the calibration. Simulations were covering a time span of 2,208 h, from the 1 Aug to 30 Oct in 2017 for case 2. Due to a partial failure of a logger in case 1, the simulation period of case 1 ended on October 12th.

The available time series of moisture content at different depths as well as temperatures were used as observations to calibrate the following parameters: $\alpha$, $n$, $\theta_s$ and $K_s$. As an initial guess for the model parameters, the values obtained in the laboratory were used (Table 1). The calibration parameters were kept homogeneous within four model layers. The choice of the four layers was based on the fact that minor differences in soil texture were presented with depth from the field sampling. The layers are 0–8, 8–30 and 30–80 cm for both cases, and 80–190 cm for case 2, and 80–305 cm for case 1. The calibration was done manually through trial and error. For the subsequent steady state simulations, to obtain the relationship between the water table vs evaporation, the average of the calibrated model parameters was used.

### Model application: lysimeter simulations and sensitivity analysis

Based on the calibrated model parameters, steady-state simulations were carried out to establish the relation between depth to groundwater and evaporation. Multiple fixed-head groundwater conditions were implemented to establish this relationship. The models were run in steady-state. In order to explore how the lysimeter-specific findings change with changing hydraulic properties of the soil, two critical parameters were chosen for a sensitivity analysis to changes (hydraulic conductivity and the van Genuchten $\alpha$). $\alpha$ was explored because it is the inverse of the air-entry pressure and therefore might play an important role in the evaporation processes. The sensitivity analysis enabled a first-order estimate of the extinction depth in the Ordos Basin at locations where no lysimeter is installed but

**Table 1** Results from the laboratory analysis

| Case | Soil depth (cm) | $\theta_s$ ($cm^3\ cm^{-3}$) | $\alpha$ ($cm^{-1}$) | $n$ | $K_s$ ($cm\ h^{-1}$) |
|---|---|---|---|---|---|
| Case 1 | 8 | 0.38 | 0.07 | 2.3 | 10 |
| | 30 | 0.37 | 0.055 | 2.1 | 13 |
| | 50 | 0.39 | 0.06 | 1.9 | 15 |
| | 100 | 0.38 | 0.055 | 1.8 | 21 |
| Case 2 | 8 | 0.39 | 0.06 | 2.2 | 13 |
| | 30 | 0.38 | 0.05 | 2.0 | 10 |
| | 50 | 0.38 | 0.05 | 2.1 | 15 |
| | 100 | 0.39 | 0.045 | 1.9 | 19 |

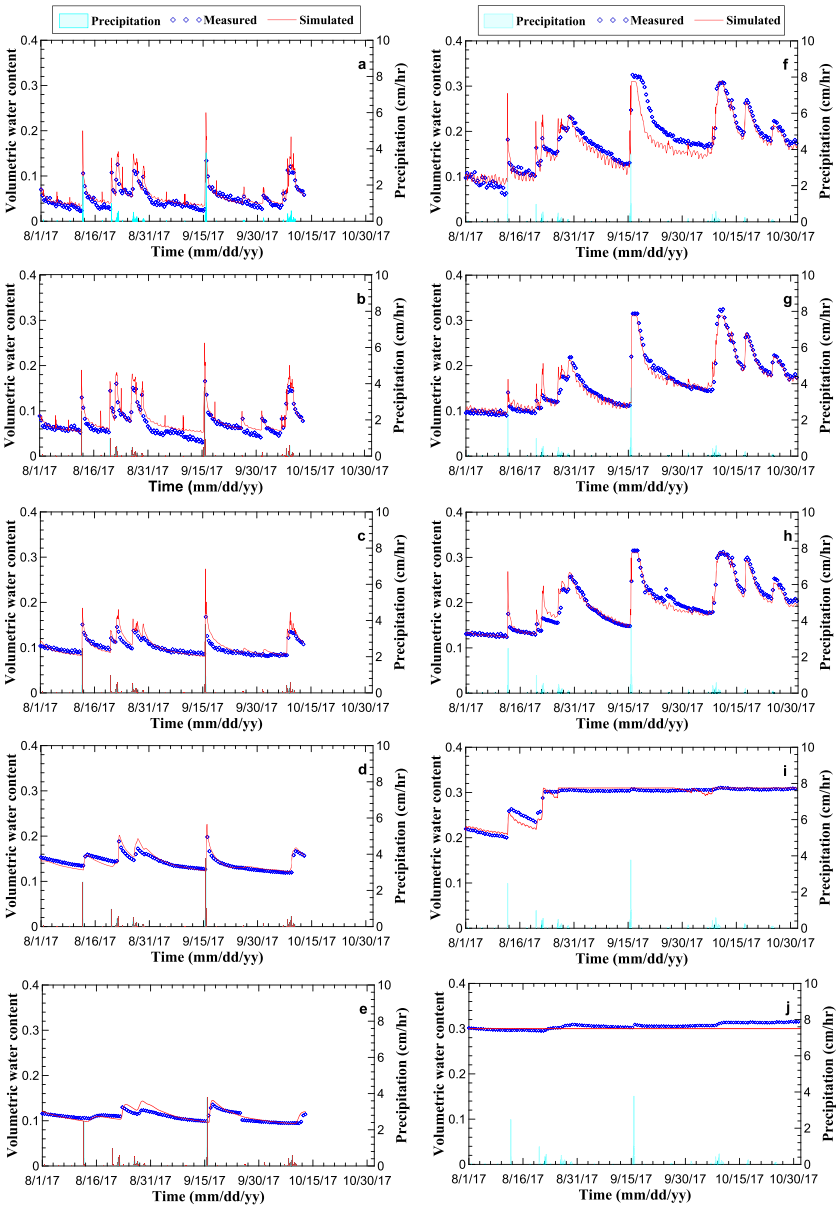


**Fig. 3** Hourly precipitation, measured soil-water content and simulated water content at **a** 3 cm, **b** 5 cm, **c** 10 cm, **d** 50 cm, **e** 100 cm of soil depth for case 1 (left panel), and at **f** 3 cm, **g** 5 cm, **h** 10 cm, **i** 50 cm, **j** 100 cm of soil depth for case 2 (right panel)

basic soil properties such as the hydraulic conductivity are available. For the cases where hydraulic conductivity was varied, $\alpha$ corresponded to the calibrated value and was kept constant. In an analogous way, for the sensitivity analysis of $\alpha$, the hydraulic conductivity was kept constant and corresponded to the calibrated

**Table 2** Evaluation of the calibration (using root mean square error (*RMSE*), mean bias error (*MBE*) and the correlation coefficient $R^2$) of soil water contents for case 1

| Statistic | Simulated vs measured water content | | | | | Simulated vs measured soil temperature | | | | |
|---|---|---|---|---|---|---|---|---|---|---|
| | Depth 3 cm | Depth 5 cm | Depth 10 cm | Depth 50 cm | Depth 100 cm | Depth 3 cm | Depth 5 cm | Depth 10 cm | Depth 50 cm | Depth 100 cm |
| RMSE | 0.011 | 0.012 | 0.011 | 0.009 | 0.007 | 2.243 | 1.879 | 1.863 | 1.174 | 1.282 |
| MBE | 0.0057 | 0.0072 | 0.003 | 0.006 | 0.002 | 0.559 | 0.340 | 0.883 | 0.973 | 1.120 |
| $R^2$ | 0.960 | 0.950 | 0.911 | 0.864 | 0.865 | 0.937 | 0.940 | 0.961 | 0.981 | 0.957 |

**Table 3** Evaluation of the calibration (using root mean square error (*RMSE*), mean bias error (*MBE*) and the correlation coefficient $R^2$) of soil water contents for case 2

| Statistic | Simulated vs measured water content | | | | | Simulated vs measured soil temperature | | | | |
|---|---|---|---|---|---|---|---|---|---|---|
| | Depth 3 cm | Depth 5 cm | Depth 10 cm | Depth 50 cm | Depth 100 cm | Depth 3 cm | Depth 5 cm | Depth 10 cm | Depth 50 cm | Depth 100 cm |
| RMSE | 0.0237 | 0.0134 | 0.0135 | 0.0076 | 0.0081 | 2.169 | 2.383 | 2.211 | 1.903 | 1.218 |
| MBE | −0.008 | −0.022 | −0.008 | 0.009 | 0.005 | 1.658 | 1.485 | 1.612 | 1.572 | 1.682 |
| $R^2$ | 0.941 | 0.976 | 0.967 | 0.947 | 0.990 | 0.972 | 0.983 | 0.966 | 0.961 | 0.986 |

value. The following values of hydraulic conductivity were used for the sensitivity analysis: 1, 10, 24, 250, 450 or 600 cm $d^{-1}$. For $\alpha$, the following values were used: 0.072, 0.066, 0.063, 0.057, 0.054 or 0.048 $cm^{-1}$.

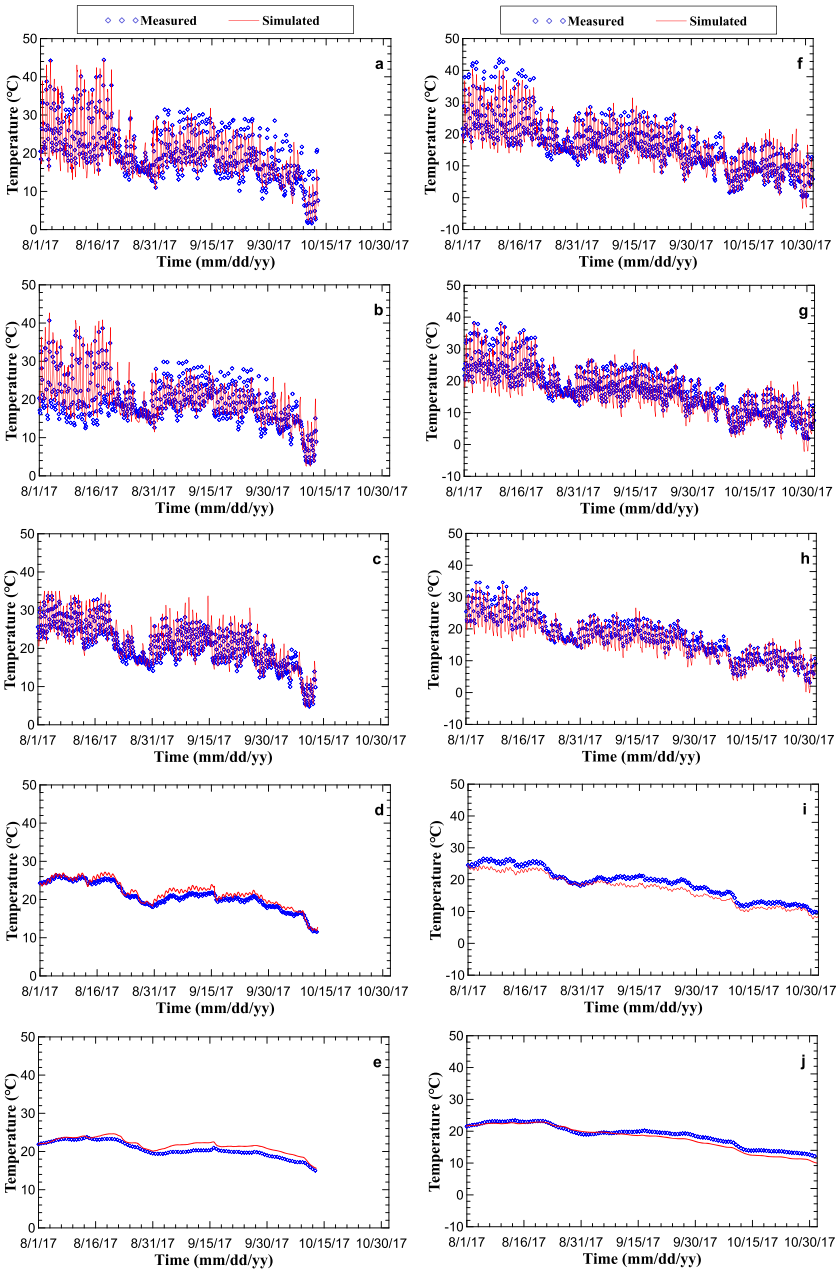


**Fig. 4** Hourly measured temperature and simulated temperature at **a** 3 cm, **b** 5 cm, **c** 10 cm, **d** 50 cm, **e** 100 cm of soil depth for case 1 (left panel), and at **f** 3 cm, **g** 5 cm, **h** 10 cm, **i** 50 cm, **j** 100 cm of soil depth for case 2 (right panel)

**Table 4** Calibrated parameters for both cases

| Case | Soil depth range (cm) | $\theta_r$(cm$^3$ cm$^{-3}$) | $\theta_s$.(cm$^3$ cm$^{-3}$) | $\alpha$ (cm$^{-1}$) | $n$ | $K_s$ (cm h$^{-1}$) |
|---|---|---|---|---|---|---|
| Case 1 | 0–8 | 0.01 | 0.30 | 0.06 | 1.9 | 8 |
| | 8–30 | 0.01 | 0.31 | 0.05 | 1.8 | 10 |
| | 30–80 | 0.01 | 0.31 | 0.04 | 1.7 | 12 |
| | 80–305 | 0.01 | 0.31 | 0.05 | 1.7 | 18 |
| Case 2 | 0–8 | 0.01 | 0.31 | 0.05 | 1.7 | 8 |
| | 8–30 | 0.01 | 0.31 | 0.045 | 1.6 | 10 |
| | 30–80 | 0.01 | 0.31 | 0.04 | 1.6 | 12 |
| | 80–190 | 0.01 | 0.30 | 0.05 | 1.6 | 15 |

## Results

### Laboratory data

Table 1 presents the laboratory data based on estimations of $\alpha$, $n$, $\theta_s$ and $K_s$. It was found that the physical properties along the soil profile were similar but not identical, and the hydraulic conductivity varied slightly. This is the reason for establishing four model layers in the upcoming calibration. The capillary fringe is approximately 50 cm.

### Calibration of model parameters

The initial model parameters resulted in an unsatisfactory fit between observed and calculated temperatures and soil moisture profiles; therefore, the model parameters in the four layers were adjusted to obtain a better fit. Volumetric soil water content ($\theta$) of two cases was simulated for 2,208 h from 1 Aug to 30 Oct in 2017. As previously discussed, the simulation period of case 1 ended on October 12th due to a problem with a sensor in one lysimeter (case 1). The values of measured rainfall, and measured and simulated volumetric soil water content at the experimental site at depths of 3, 5, 10, 50 and 100 cm on different days are shown in Fig. 3. The statistics of measured and simulated volumetric water content are compared in Tables 2 and 3. The average RMSE and $R^2$ values of the soil water content at the five depths were 0.01 cm$^3$ cm$^{-3}$ and 0.91 for case 1, and 0.013 cm$^3$ cm$^{-3}$ and 0.96 for case 2. Figure 4 shows the measured and simulated temperatures for cases 1 and 2. The calibrated parameters that were used to obtain these simulations are provided in Table 4.

To illustrate the importance of an explicit simulation of vapor, a detailed analysis of daily liquid water and vapor fluxes in the upper layer was carried out and is illustrated for two specific days (August 10th–11th) in Fig. 5. On a daily time-scale, the water vapor flux was negative from 9:00 to 21:00 at a depth of 15 cm (negative values signify a downward flux), and positive at other times in both cases. For both cases, the vapor flux was negative at a depth of 22 cm at around 11:00–23:00. In addition, the minimum and maximal vapor fluxes occurred at 15:00 and 6:00 in both cases. Similar results have also been obtained by Zhang et al. (2018).

The calibrated models were subsequently used to explore the relationship between depth to groundwater and evaporation rates. The results are shown in Fig. 6. Several interesting points can be identified. For water tables above 52-cm depth, the contribution of groundwater to evaporation is independent of the depth to the water table. After the water table falls further, a rapid decline in contribution can be observed. The extinction depth is around 105 cm: If the water table falls below this depth, capillary rise can no longer sustain evaporation.

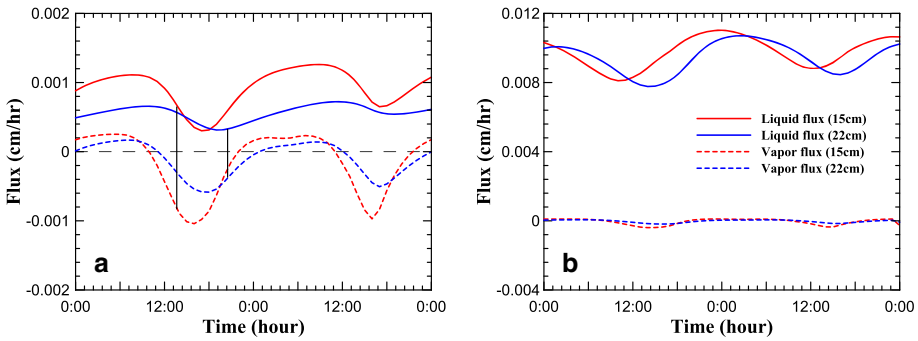


**Fig. 5** Diurnal liquid water flux and vapor flux near the ground surface using the Hydrus-1 D model for two selected days (10 and 11 Aug) for **a** case 1 and **b** case 2. The legend in **b** applies to **a**

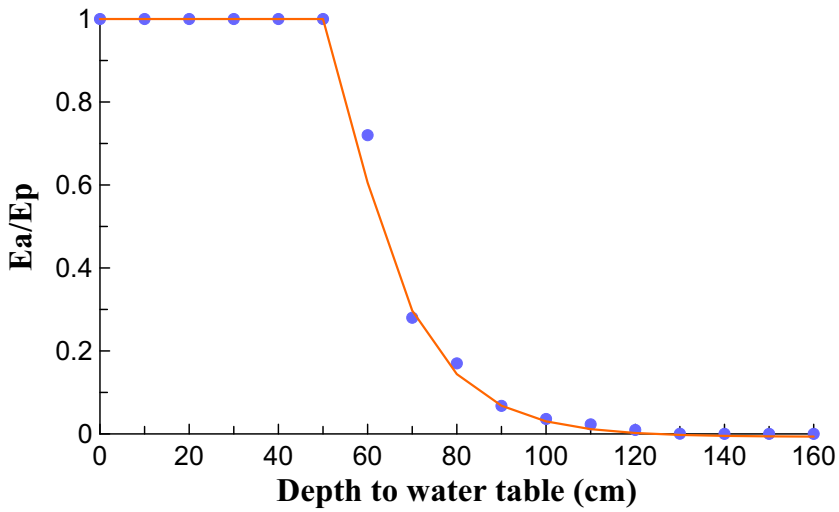


**Fig. 6** Ratio between actual evapotranspiration (Ea) and potential evaporation (Ep) for different water-table depths

Based on the model simulations, the following relation between depth to groundwater (DTG) and evaporation rates can be defined for the lysimeter site in the Ordos Basin:

$$\frac{E_a}{E_p} = \begin{cases} 1 & \text{for DTG} < 51.3 \text{ cm} \\ -0.008 + e^{-0.007(\text{DTG}-51.3)} & \text{for } 51.3 \text{ cm} < \text{DTG} < 105 \text{ cm} \\ 0 & \text{for DTG} > 105 \text{ cm} \end{cases} \quad (12)$$

## Sensitivity analysis

The results of the sensitivity analysis are shown in Fig. 7. An important dependency between hydraulic conductivity and the relation between depth to groundwater and evaporation rates, as well as the resulting extinction depth, is observed. Lower values of hydraulic conductivity result in smaller

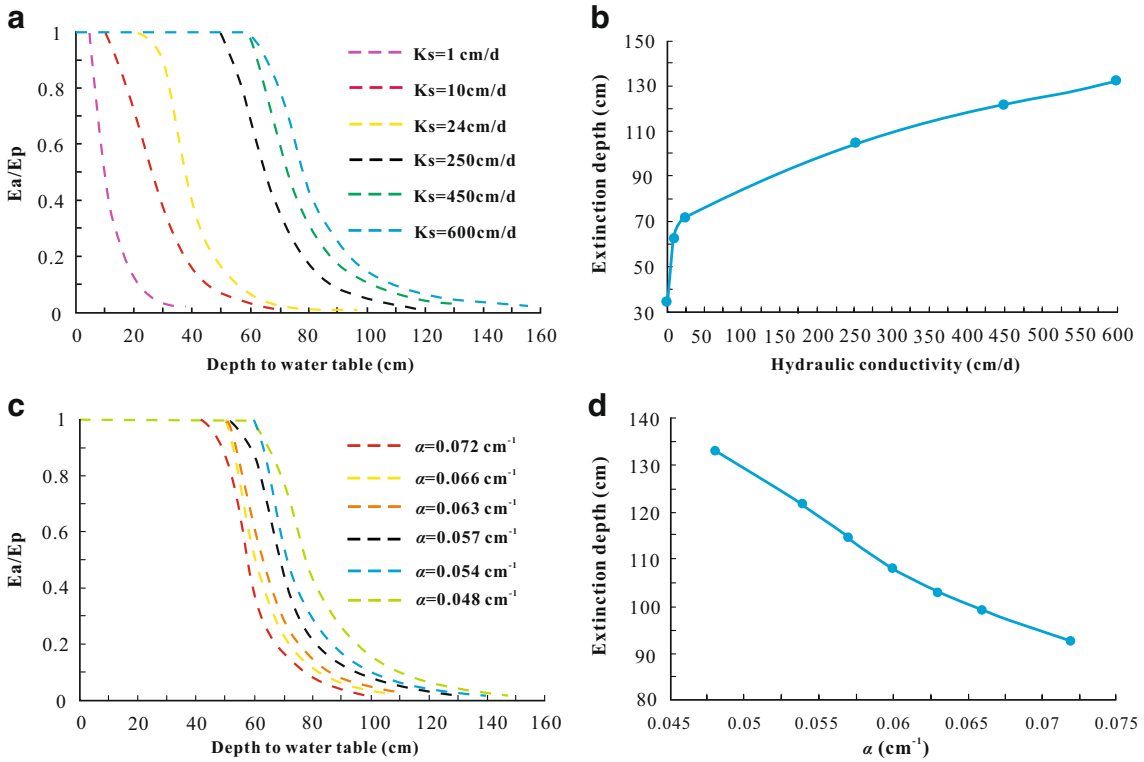


**Fig. 7** **a** The ratio between actual (Ea) and potential (Ep) evaporation as a function of water-table depth for different hydraulic conductivities; **b** the relationship between hydraulic conductivity and extinction depth; **c** the ratio between actual (Ea) and potential (Ep) evaporation with water-table depth for changing $\alpha$; and **d** the relationship between $\alpha$ and extinction depth

extinction depths and a comparably rapid decline of the evaporation rate with decreasing water tables. This is not unexpected as smaller hydraulic conductivities constitute a higher resistance to flow and therefore reduce the capillary upwards flux. If hydraulic conductivities were smaller than 10 cm $d^{-1}$, evaporation rates drop immediately with a declining water table, while for larger conductivities, actual evapotranspiration (ET) rates correspond to potential rates down to a depth to groundwater of over 60 cm. The importance of variations of $\alpha$ are less pronounced than the hydraulic conductivities. Increasing values of $\alpha$ cause a decrease of the extinction depth.

## Discussion and conclusions

Water resources management in arid and semi-arid areas such as the Ordos Basin requires careful consideration of groundwater evaporation. In this regard, it is important to develop a quantitative relation between depth to groundwater and evaporation rates. Such relationships and the associated extinction depths have been developed for a wide range of soil types and are widely implemented in numerical models. Linear or quadratic decay functions are frequently used in modelling approaches (e.g. in MODFLOW) to describe the relationship between water-table depth and evaporation rates. The relation found for this specific site differs slightly from other approaches. At the field site, the evaporation rates are independent of the water table until depths of 52 cm. If the water table is above this critical depth, very high evaporation losses are expected which can contribute to soil salinization and degradation. It is also important to note that these evaporation fluxes are unproductive and constitute a loss of water resources without any benefit. On the other hand, evaporation rates decline rapidly if the water table drops below 52 cm. The extinction depth of 105 cm is comparable to the extinction depth reported in the literature for such soil materials (e.g. Shah et al. 2007. It is noteworthy that the extinction depth found in this study corresponds to approximately twice the height of the capillary fringe.

The numbers above are related to the materials presented in the lysimeter. While the most commonly found soil type in the Ordos Basin is sand with these properties (Table 1), variations of hydraulic conductivities between 50 and 400 cm $d^{-1}$ occur. In relative terms, smaller variations of $\alpha$ are present. Given that the materials in the lysimeter are representing a large portion of the Ordos Basin, the relation established in Eq. (12) can be used as a first approximation for relating evaporation rates to the depth to groundwater. If differences in hydraulic conductivities and $\alpha$ are expected, it is recommended to measure them and use this information in combination with Fig. 7 for the estimation of the extinction depth. Note that if significantly different soil types are present, and therefore the soil retention function is significantly different, the findings reported here should not be used without additional simulations or lysimeter experiments—for example, the relative importance of $\alpha$ is expected to increase for smaller hydraulic conductivities.

In terms of the methodological approach chosen, the combination of lysimeter data and a comprehensive numerical model was useful because it allows to systematically explore the relationship between depth to groundwater and evaporation. Given the importance of vapor transport in simulating evaporation in arid and semi-arid regions, the relatively high complexity of the modelling approach was an appropriate choice. The calibration of the model was done manually, which makes a comprehensive uncertainty analysis difficult. The fit between observed and simulated quantities was good and deemed sufficient for the subsequent analysis; however, a comprehensive uncertainty analysis of the model results is recommended for follow-up research. Nevertheless, the identified relations between water-table depth and evaporation constitutes important information to the local government responsible for managing soil and water resources.

**Acknowledgements** We greatly appreciate the constructive feedback and comments from the three reviewers and the editor.

**Funding information** This research was supported by the National Natural Science Foundation of China (Nos. U1603243, 41230314).

## References

Allen RG, Pereira LS, Raes D, Smith M (1998) Crop evapotranspiration: guidelines for computing crop water requirements, FAO Irrigation and Drainage Paper no. 56. FAO, Rome

An K, Wang W, Zhao Y, Huang W, Chen L, Zhang Z, Wang Q, Li W (2016) Estimation from soil temperature of soil thermal diffusivity and heat flux in sub-surface layers. Boundary-Layer Meteorol 158(3):473–488. https://doi.org/10.1007/s10546-015-0096-7

An K, Wang W, Wang Z, Zhao Y, Yang Z, Chen L, Zhang Z, Duan L (2017) Estimation of ground heat flux from soil temperature over a bare soil. Theoretic Appl Climatol 129(3–4):913–922. https://doi.org/10.1007/s00704-016-1816-8

Assouline S, Tyler SW, Selker JS, Lunati I, Higgins CW, Parlange MB (2013) Evaporation from a shallow water table: diurnal dynamics of water and heat at the surface of drying sand. Water Resour Res 49: 4022–4034. https://doi.org/10.1002/wrcr.20293

Baldocchi DD, Xu L (2007) What limits evaporation from Mediterranean oak woodlands, the supply of moisture in the soil, physiological control by plants or the demand by the atmosphere? Adv Water Resour 30(10):2113–2122. https://doi.org/10.1016/j.advwatres.2006.06.013

Balugani E, Lubczynski MW, Metselaar K (2016) A framework for sourcing of evaporation between saturated and unsaturated zone in bare soil condition. Int Assoc Sci Hydrol Bull 61(11):1981–1995. https://doi.org/10.1080/02626667.2014.966718

Balugani E, Lubczynski MW, Reyes-Acosta L, dTC V, Francés AP, Metselaar K (2017) Groundwater and unsaturated zone evaporation and transpiration in a semi-arid open woodland. J Hydrol 547:54–66. https://doi.org/10.1016/j.jhydrol.2017.01.042

Banimahd SA, Zand-Parsa S (2013) Simulation of evaporation, coupled liquid water, water vapor and heat transport through the soil medium. Agric Water Manag 130:168–177. https://doi.org/10.1016/j.agwat.2013.08.022

Brunner P, Li HT, Kinzelbach W, Li WP (2007) Generating soil electrical conductivity maps at regional level by integrating measurements on the ground and remote sensing data. Int J Remote Sens 28(15): 3341–3361. https://doi.org/10.1080/01431160600928641

Brunner P, Li HT, Kinzelbach W, Li WP, Dong XG (2008) Extracting phreatic evaporation from remotely sensed maps of evapotranspiration. Water Resour Res 44:1291–1295. https://doi.org/10.1029/2007WR006063

Brutsaert W (2014) The daily mean zero flux plane during soil controlled evaporation: a Green's function approach. Water Resour Res 50(12): 9405–9413. https://doi.org/10.1002/2014WR016111

Chen L, Wang W, Zhang Z, Wang Z, Wang Q, Zhao M, Gong C (2018) Estimation of bare soil evaporation for different depths of water table in the wind-blown sand area of the Ordos Basin, China. Hydrogeol J 4:1–12. https://doi.org/10.1007/s10040-018-1774-6

Chung SO, Horton R (1987) Soil heat and water flow with a partial surface mulch. Water Resour Res 23:2175–2186. https://doi.org/10.1029/WR023i012p02175

de Vries DA (1958) Simultaneous transfer of heat and moisture in porous media. Trans Am Geophys Union 39:2175–2186

de Vries DA (1963) The thermal properties of soils, In Physics of Plant Environment, edited by R. W. van Wijk, pp. 210-235, North Holland, Amsterdam

Doble RC, Crosbie RS (2017) Review: current and emerging methods for catchment-scale modelling of recharge and evapotranspiration from shallow groundwater. Hydrogeol J 25:3–23. https://doi.org/10.1007/s10040-016-1470-3

Doble R, Simmons C, Jolly I, Walker G (2006) Spatial relationships between vegetation cover and irrigation-induced groundwater discharge on a semi-arid floodplain, Australia. J Hydrol 329:75–97. https://doi.org/10.1016/j.jhydrol.2006.02.007

Doble RC, Pickett T, Crosbie RS, Morgan LK, Turnadge C, Davies PJ (2017) Emulation of recharge and evapotranspiration processes in shallow groundwater systems. J Hydrol 555:894–908. https://doi.org/10.1016/j.jhydrol.2017.10.065

Fahle M, Dietrich O (2014) Estimation of evapotranspiration using diurnal groundwater level fluctuations: comparison of different approaches with groundwater lysimeter data. Water Resour Res 50(1):273–286. https://doi.org/10.1002/2013WR014472

Gardner WR (1958) Some steady state solutions of the unsaturated moisture flow equation with application to evaporation from a water table. Soil Sci 85:228–232. https://doi.org/10.1097/00010694-195804000-00006

Gardner WR, Fireman M (1958) Laboratory studies of evaporation from soil columns in the presence of a water table. Soil Sci 85(5):244–249. https://doi.org/10.1097/00010694-195805000-00002

Gowing JW, Konukcu F, Rose DA (2006) Evaporative flux from a shallow water table: the influence of a vapour–liquid phase transition. J Hydrol 321:77–89. https://doi.org/10.1016/j.jhydrol.2005.07.035

Hernández-López MF, Gironás J, Braud I, Suárez F, Muñoz JF (2014) Assessment of evaporation and water fluxes in a column of dry saline soil subject to different water table levels. Hydrol Process 28:3655–3669. https://doi.org/10.1002/hyp.9912

Hillel D (1998) Entry of water into soil. In: Environmental soil physics. Academic, San Diego, pp 385–426

Huang J, Zhou Y, Hou R, Wenninger J (2015) Simulation of water use dynamics by Salix bush in a semiarid shallow groundwater area of the Chinese Erdos plateau. Water 7:6999–7021. https://doi.org/10.3390/w7126671

Johnson JE, Yáñez J, Ortiz C, Muñoz J (2010) Evaporation from shallow groundwater in closed basins in the Chilean Altiplano. Hydrol Sci J 55(4):624–635

Kamai T, Assouline S (2018) Evaporation from deep aquifers in arid regions: analytical model for combined liquid and vapor water fluxes. Water Resour Res 54. https://doi.org/10.1029/2018WR023030

Kamai T, Weisbrod N, Dragila MI (2009) Impact of ambient temperature on evaporation from surface-exposed fractures. Water Resour Res 45(2):325–336. https://doi.org/10.1029/2008WR007354

Lehmann P, Assouline S, Or D (2008) Characteristic lengths affecting evaporative drying of porous media. Phys Rev E Stat Nonlinear Soft Matter Phys 77:056309. https://doi.org/10.1103/PhysRevE.77.056309

Li HT, Kinzelbach W, Brunner P, Li WP, Dong XG (2008) Topography representation methods for improving evaporation simulation in groundwater modeling. J Hydraul 356:1–2

Liu T, Liu L, Luo Y, Lai J (2015) Simulation of groundwater evaporation and groundwater depth using SWAT in the irrigation district with shallow water table. Environ Earth Sci 74:315–324. https://doi.org/10.1007/s12665-015-4034-2

Milly PCD (1982) Moisture and heat transport in hysteretic, inhomogeneous porous media: a matric head-based formulation and a numerical model. Water Resour Res 18:489–498. https://doi.org/10.1029/WR018i003p00489

Nazarieh F, Ansari H, Ziaei AN, Izady A, Davari K, Brunner P (2018) Spatial and temporal dynamics of deep percolation, lag time and recharge in an irrigated semi-arid region. Hydrogeol J. https://doi.org/10.1007/s10040-018-1789-z

Nimmo JR, Deason JA, Izbicki JA, Martin P (2002) Evaluation of unsaturated zone water fluxes in heterogeneous alluvium at a Mojave Basin site. Water Resour Res 38(10):1215. https://doi.org/10.1029/2001WR000735

Philip JR (1957) Evaporation, and moisture and heat fields in the soil. J Meteorol 14:354–366. https://doi.org/10.1175/1520-0469(1957)014<0354:eamahf>2.0.co;2

Philip JR, de Vries DA (1957) Moisture movement in porous materials under temperature gradients. Trans Am Geophys Union 38(2):222–232

Ripple CD, Rubin J, Van Hylckama TEA (1970) Estimating steady-state evaporation rates from bare soils under conditions of high water table. http://pubs.er.usgs.gov/publication/70047724. Accessed June 2019

Sadeghi M, Shokri N, Jones SB (2012) A novel analytical solution to steady-state evaporation from porous media. Water Resour Res 48(9):9516. https://doi.org/10.1029/2012WR012060

Saito H, Šimůnek J, Mohanty BP (2006) Numerical analysis of coupled water vapor, and heat transport in the vadose zone. Vadose Zone J 5: 784–800. https://doi.org/10.2136/vzj2006.0007

Salvucci GD (1997) Soil and moisture independent estimation of stage-2 evaporation from potential evaporation and albedo or surface temperature. Water Resour Res 33(1):111–122. https://doi.org/10.1029/96WR02858

Scanlon BR, Keese K, Reedy RC, Simunek J, Andraski BJ (2003) Variations in flow and transport in thick desert vadose zones in response to paleoclimatic forcing (0–90 kyr): field measurements, modeling, and uncertainties. Water Resour Res 39(7):1179. https://doi.org/10.1029/2002WR001604

Selim T, Bouksila F, Berndtsson R, Persson M (2013) Soil water and salinity distribution under different treatments of drip irrigation. Soil Sci Soc Am J 77:1144–1156. https://doi.org/10.2136/sssaj2012.0304

Selker JS (2017) Analytical estimation show low depth-independent water loss due to vapor flux from deep aquifers. Water Resour Res 53(6):4562–4563. https://doi.org/10.1002/2017WR021014

Shah N, Nachabe M, Ross M (2007) Extinction depth and evapotranspiration from ground water under selected land covers. Ground Water 45:329–338

Shang H, Wang W, Dai Z, Duan L, Zhao Y, Zhang J (2016) An ecology-oriented exploitation mode of groundwater resources in the northern Tianshan Mountains, China. J Hydrol 543:386–394. https://doi.org/10.1016/j.jhydrol.2016.10.012

Simunek J (2005) The Hydrus-1D software package for simulating the movement of water, heat, and multiple solutes in variably saturated media. HYDRUS Software Series 1, HYDRUS, https://www.pc-progress.com/en/Default.aspx?h3d-ver2. Accessed June 2019

Simunek J, van Genuchten MT, Sejna M (2008) Development and applications of the HYDRUS and STANMOD software packages and related codes. Vadose Zone J 72(9):587–600. https://doi.org/10.2136/vzj2007.0077

Song W, Cui Y, Tang AM, Ding W, Tran TD (2014) Experimental study on water evaporation from sand using environmental chamber. Adv Water Sci 51(2):115–128. https://doi.org/10.1139/cgj-2013-0155

Soylu M, Istanbulluoglu E, Lenters J, Wang T (2011) Quantifying the impact of groundwater depth on evapotranspiration in a semi-arid grassland region. Hydrol Earth Syst Sci 15:787–806

Talsma T (1963) The control of saline groundwater. Mededelingen Landbouwhogeschool, Wageningen, The Netherlands, 68 pp. http://edepot.wur.nl/185086. Accessed June 2019

Van Genuchten MT (1980) A closed form equation for predicting the hydraulic conductivity of unsaturated soils. Soil Sci Soc Am J 44(5):892–898. https://doi.org/10.2136/sssaj1980.03615995004400050002x

Walvoord MA, Plummer MA, Phillips FM, Wolfsberg AV (2002) Deep arid system hydrodynamics 1: equilibrium states and response times in thick desert vadose zones. Water Resour Res 38(12):1308. https://doi.org/10.1029/2001WR000824

Wang W, Li Y, Yang F, Hou L, Zhao G, Li J (2011a) Experimental and numerical study of coupled flow and heat transport. Water Manag 164:533–547. https://doi.org/10.1680/wama.10.00088

Wang W, Li J, Feng X, Chen X, Yao K (2011b) Evolution of stream–aquifer hydrologic connectedness during pumping: experiment. J Hydrol 402:401–414. https://doi.org/10.1016/j.jhydrol.2011.03.033

Wang W, Zhang Z, Yeh TCJ, Qiao G, Wang W, Duan L, Huang SY, Wen JC (2017) Flow dynamics in vadose zones with and without vegetation in an arid region. Adv Water Resour 106. https://doi.org/10.1016/j.advwatres.2017.03.011

Yamanaka T, Yonetani T (1999) Dynamics of the evaporation zone in dry sandy soils. J Hydrol 217(1–2):135–148. https://doi.org/10.1016/S0022-1694(99)00021-9

Zhang Z, Wang W, Wang Z, Chen L, Gong C (2018) Evaporation from bare ground with different water-table depths based on an in-situ experiment in Ordos plateau, China. Hydrogeol J 26:1683–1691. https://doi.org/10.1007/s10040-018-1751-0

Zhang Z, Wang W, Gong C, Wang Z, Duan L, Yeh TCL, Yu P (2019) Evaporation from seasonally frozen bare and vegetated ground at various groundwater table depths in the Ordos Basin, Northwest China. Hydrol Process. https://doi.org/10.1002/hyp.13404